Polyfluorenes Containing Dibenzo[*a,c*]phenazine Segments: Synthesis and Efficient Blue Electroluminescence from Intramolecular Charge Transfer States

Yan Zhu, Katherine M. Gibbons, Abhishek P. Kulkarni, and Samson A. Jenekhe*

Department of Chemical Engineering and Department of Chemistry, University of Washington, Seattle, Washington 98195-1750

Received October 23, 2006; Revised Manuscript Received December 7, 2006

ABSTRACT: Five new conjugated copolymers of 9,9′-dioctylfluorene and dibenzo[*a,c*]phenazine were synthesized by Suzuki copolymerization and were used to achieve efficient blue electroluminescence (EL) from intramolecular charge-transfer excited states. The copolymers had moderate molecular weights (M_w = 31 250−71 120, M_w/M_n = 2.06−3.48) and enhanced glass-transition temperature of 68−130 °C. Intramolecular charge transfer (ICT) between the fluorene and dibenzo[*a,c*]phenazine moieties dominated the ground and excited-state electronic structures of the copolymers, as evidenced by the new low-energy absorption band and the strong positive solvatochromism in photoluminescence (PL). The copolymers emitted blue light in dilute toluene solutions with PL quantum yields of 43−80% as the composition was varied from 2 to 20 mol % dibenzo[*a,c*]phenazine. Blue EL from ICT excited states of the copolymers was achieved in light-emitting diodes (LEDs) with luminances of 1260−4600 cd/m^2 and external quantum efficiencies of 0.47−2.89% (at >100 cd/m^2), depending on the copolymer composition. Besides their excellent stability as blue emitters, the fluorene−dibenzo[*a,c*]phenazine copolymer LEDs were substantially better than the polyfluorene homopolymer diodes. These results show that efficient blue electroluminescence can be achieved from the intramolecular charge-transfer emission of a conjugated donor−acceptor copolymer, leading to blue LEDs with enhanced performance compared to poly(9,9-dialkylfluorene)s.

Introduction

Polyfluorenes and fluorene-containing copolymers have attracted considerable attention as active materials in organic electronic devices[1−6] such as light-emitting diodes (LEDs),[1−4] photovoltaic cells,[5a,b] and field-effect transistors (FETs).[6a,b] Polyfluorenes are currently widely explored as the emissive materials in polymer light-emitting diodes because of their high photoluminescence (PL) efficiency, good film-forming, and hole-transporting properties.[1−4] To obtain high quantum efficiency LEDs, balanced charge injection and transport of both holes and electrons in the emissive material is necessary. However, poly(9,9′-dialkylfluorene)s such as poly(9,9′-dioctylfluorene) (PFO) is a p-type (electron donor), blue-emitting polymer with a large band gap (∼3.1 eV) and a low electron affinity (EA = 2.5 eV).[2c] PFO has good hole-transport properties, with mobility of holes on the order 10^{-3} cm^2/Vs;[6b] electron transport is, however, poor. To improve the electron transport properties and achieve balanced charge carrier injection/transport in polyfluorenes, a common strategy is to incorporate n-type (electron acceptor) comonomers into the predominantly p-type polyfluorene backbone. Polyfluorene copolymers have been reported, with emission colors spanning the entire visible spectrum.[2a,b,4]

Introduction of donor−acceptor (D−A) moieties on a conjugated polymer backbone often results in intramolecular charge transfer (ICT)[7] between the donor and acceptor moieties. Significant changes in the electronic structures of the parent homopolymers often result from such a donor−acceptor copolymer architecture, leading to small band gaps,[5,7] broad absorption bands with near-infrared absorption,[5,7] and ambipolar charge transport[6f], which have attracted much interest for applications in photovoltaic cells[5] and thin film transistors.[6]

Chart 1

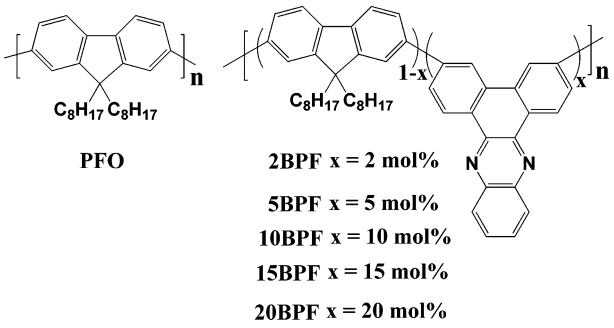

There are few reports on ICT-based electroluminescence in polyfluorenes and other emissive D−A copolymers.[4c,8] High-performance OLEDs based on ICT emission from D−A small molecules and oligomers have been previously reported.[9,10] Red and near-infrared electroluminescence from ICT excited states was observed in two phenylenevinylene-based D−A copolymers.[8b] Several copolymers consisting of dihexylfluorene and various electron acceptors were prepared and the effect of ICT on the emission color of these copolymers was recently reported.[4c] Many factors, such as the strength of the ICT, D−A copolymer composition, and chain architecture, can be expected to strongly effect the electronic structures and the electroluminescence of D−A copolymers. The structure−property relationships in emissive D−A copolymers remain to be fully understood.

Many n-type building blocks such as oxadiazole,[11a] quinoline,[11b] pyridine,[11c] and quinoxaline,[3e] have been incorporated into polyfluorene main chain or as pendants attached at the C-9 position of fluorene unit to improve electron injection and transport properties or to tune the emission color. Our motivation for the present work is to synthesize polyfluorene copolymers with improved electron injection/transport properties while retaining blue emission by introducing a strong electron

* Corresponding author. E-mail: jenekhe@u.washington.edu.

10.1021/ma062445z CCC: $37.00
Published on Web 01/19/2007

Scheme 1

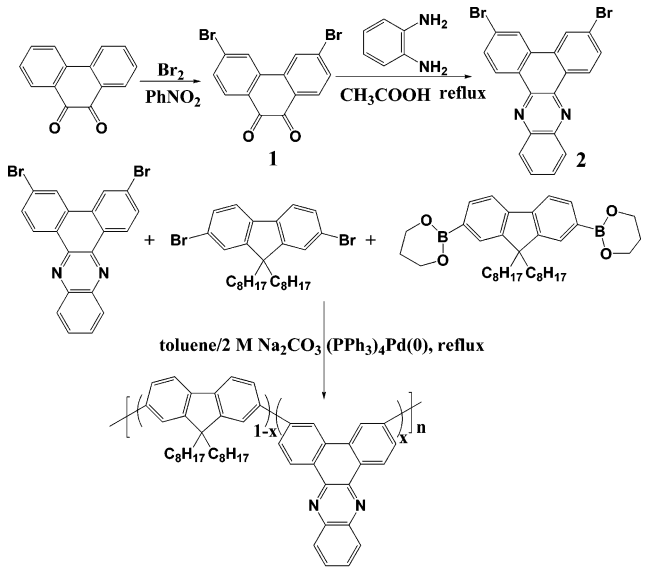

acceptor, dibenzo[*a*,*c*]phenazine, into the polyfluorene backbone and to systematically investigate the effects of the concentration of the n-type comonomer on the ICT excited-state processes relevant to the electroluminescence of the copolymers. We chose dibenzo[*a*,*c*]phenazine as the n-type moiety because it is a stronger electron acceptor with a half-wave reduction potential ($E_{1/2}^{red}$) of −1.35 V vs Ag/Ag^+ compared to other extensively investigated n-type moieties such as quinoxaline ($E_{1/2}^{red} = -1.80$ V vs Ag/Ag^+) and quinoline ($E_{1/2}^{red} = -2.18$ V vs Ag/Ag^+).[12] Dibenzo[*a*,*c*]phenazine has not previously been explored at all as an n-type building block in organic or polymer semiconductors. Furthermore, higher thermal stability of fluorene−dibenzo[*a*,*c*]phenazine copolymers can be expected because dibenzo[*a*,*c*]phenazine is a very rigid moiety with a fused pentacyclic ring system.

In this paper, we report the synthesis and intramolecular charge-transfer blue electroluminescence of a series of five new fluorene copolymers containing dibenzo[*a*,*c*]phenazine as an electron acceptor (n-type) moiety. Effects of the ICT between fluorene donor and dibenzo[*a*,*c*]phenazine acceptor on the photophysics and electroluminescence of the copolymers were systematically studied by varying the concentration of the n-type moiety. A series of polyfluorene copolymers containing 2, 5, 10, 15, and 20 mol % dibenzo[*a*,*c*]phenazine, denoted 2BPF, 5BPF, 10BPF, 15BPF, and 20BPF (Chart 1), respectively, was synthesized by Suzuki polymerization. Systematic trends in the variation of relevant copolymer properties such as the glass-transition temperature (T_g), and PL quantum yields were observed. Strong ICT in the fluorene−dibenzophenazine copolymers was observed both in the optical absorption and in the PL emission spectra. Efficient blue electroluminescence from ICT excited states of the BPF copolymers was achieved with brightness as high as 4600 cd/m^2, and EL external quantum efficiency and luminous efficiency as high as 2.89% (at >100 cd/m^2) and 2.69 cd/A, respectively.

Results and Discussion

Synthesis and Characterization. The synthetic routes used to prepare the monomer and polymers are outlined in Scheme 1. The condensation of 3,6-dibromo-phenanthrene-9,10-dione (**1**) with 1,2-phenylenediamine afforded the monomer 3,6-dibromo-dibenzo[*a*,*c*]phenazine (**2**) in high yield (90%).[13]

Table 1. Molecular Weights and Thermal Properties of Polymers

polymer	M_n[a]	M_w/M_n[a]	T_g[b] (°C)	T_d[c] (°C)
PFO	21 600	2.09	66	407
2BPF	25 130	2.82	68	401
5BPF	23 640	2.06	70	403
10BPF	19 130	2.62	87	403
15BPF	13 830	2.97	108	413
20BPF	8980	3.48	130	412

[a] Molecular weights were determined by GPC using polystyrene standards. [b] Glass-transition temperature estimated from second-heating DSC curve. [c] Onset decomposition temperature measured from TGA under nitrogen.

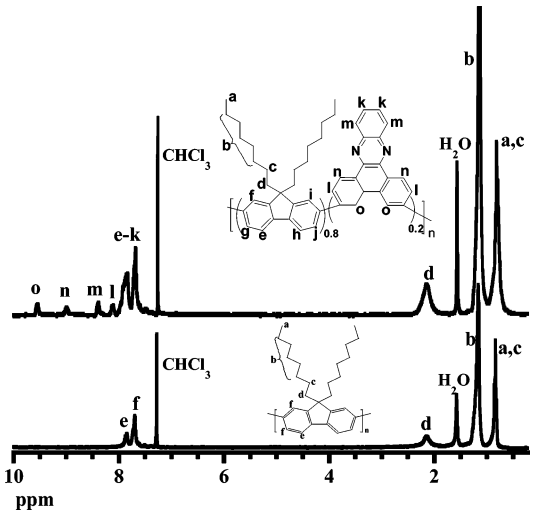

Figure 1. ^{1}H NMR spectra of PFO homopolymer and 20BPF copolymer.

Random poly(9,9-dioctylfluorene-*co*-dibenzo[*a*,*c*]phenazine-3,6-diyl) (BPF) copolymers and the corresponding polyfluorene homopolymer, poly(9,9′-dioctylfluorene) (PFO) were synthesized by Suzuki coupling polymerization. The molar ratio of dibenzo[*a*,*c*]phenazine moiety in the copolymers was controlled by adjusting the molar ratio between 9,9′-dioctyl-2,7-dibromofluorene and 3,6-dibromo-dibenzo[*a*,*c*]phenazine while maintaining a 1:1 molar ratio between the dibromides and the bis(trimethylene boronate). All the copolymers were soluble in organic solvents such as toluene, chloroform, and tetrahydrofuran (THF). The number-average molecular weights (M_n) of these polymers were determined by gel permeation chromatography (GPC) against polystyrene standards in THF to be 8980 to 25 130 with a polydispersity index of 2.06−3.48 (Table 1).

The chemical structures of the copolymers were verified by ^{1}H NMR and FT−IR spectra. The ^{1}H NMR spectra of the copolymers and PFO homopolymer were in good agreement with the proposed structures. Representative ^{1}H NMR spectra of copolymer 20BPF and PFO homopolymer are shown in Figure 1. The small peaks at 9.55, 9.00, 8.39, and 8.11 ppm, which are due to the protons (labeled "o", "n", "m", and "l", respectively, in Figure 1) in the dibenzo[*a*,*c*]phenazine unit, were observed in the spectra of all the copolymers and were absent in the spectrum of PFO. The multiple peaks in the range of 7.68−7.86 ppm correspond to the other aromatic protons in the dibenzo[*a*,*c*]phenazine and fluorene units. The resonances at 2.15, 1.14, and 0.80 ppm are assigned to the aliphatic protons in the octyl side chains. FT−IR spectra of the copolymers and PFO also confirmed their molecular structures. Representative FT−IR spectra of copolymer 20BPF and PFO are shown in Figure 2. Compared to the PFO homopolymer, the new vibrational bands at 1607 and 1532 cm^{-1} in all the copolymers

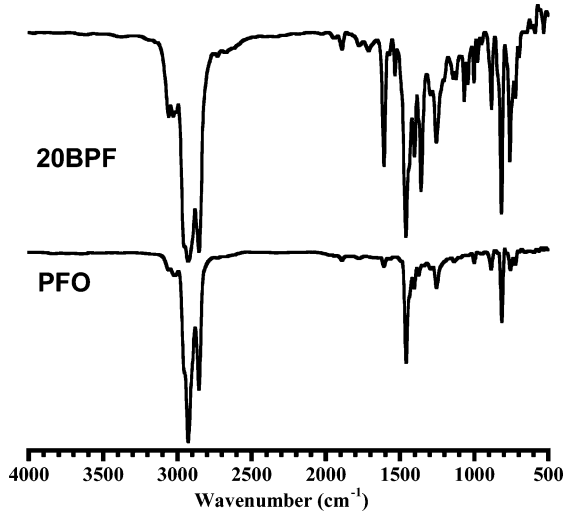

Figure 2. FT−IR spectra of PFO homopolymer and 20BPF copolymer.

are assigned to the stretching vibrations of the C═N group in the dibenzo[*a*,*c*]phenazine ring.

The thermal properties of the polymers were evaluated by thermogravimetric analysis (TGA) and differential scanning calorimetry (DSC), and the results are summarized in Table 1. TGA revealed that the onset decomposition temperatures of the copolymers and PFO homopolymer under nitrogen were in the range of 401−413 °C, indicative of good thermal stability. PFO homopolymer exhibits three thermal transitions: a glass-transition temperature (T_g = 66 °C), a crystallization exothermic peak (90 °C), and a melting peak (150 °C) (not shown). These typical thermal characteristics in PFO are similar to previous reports by our group and others.[3e,14] Similar thermal transitions were observed for copolymer 2BPF. However, the DSC traces of all the other copolymers containing greater than 2 mol % dibenzo[*a*,*c*]phenazine showed no crystallization or melting peaks, but only glass transitions. The T_g of these copolymers are in the range of 66−130 °C, increasing steadily with the composition of dibenzo[*a*,*c*]phenazine moiety in the copolymers, from 66 °C in PFO to 130 °C in 20BPF. This clearly indicates that the incorporation of the rigid dibenzo[*a*,*c*]phenazine unit into the polyfluorene backbone reduces the segmental mobility and effectively suppresses the tendency of the polymer chains to densely pack and crystallize. We note that the T_g of fluorene−dibenzo[*a*,*c*]phenazine copolymer is higher than that of fluorene−quinoxaline copolymer with the same composition of the n-type unit,[3e] confirming that dibenzo[*a*,*c*]phenazine is a more rigid moiety compared to quinoxaline.

Photophysical Properties. The normalized optical absorption spectra of PFO and the five BPF copolymers in dilute (10^{-5} M) toluene solutions are shown in Figure 3a. With increasing fraction of dibenzo[*a*,*c*]phenazine in the copolymers, the main absorption band becomes broader and progressively blue-shifts from 387 nm in PFO homopolymer to 378 nm in 20BPF. This absorption band is associated with the $\pi-\pi^*$ transition of the polyfluorene backbone.[1a] A new absorption band at 423 nm is seen in the copolymers, and it increases in intensity with increasing dibenzophenazine amount from 2BPF to 20BPF. We note that the absorption spectrum of the monomer, 3,6-dibromodibenzo[*a*,*c*]phenazine in dilute toluene solution (not shown) shows peaks at 380 and 400 nm and no absorption above 410 nm. Thus, the 423 nm band in the copolymers cannot be assigned to the isolated dibenzo[*a*,*c*]phenazine moieties. An absorption band at 436 nm due to aggregation has previously been observed in highly concentrated (10 mg/mL) solutions of

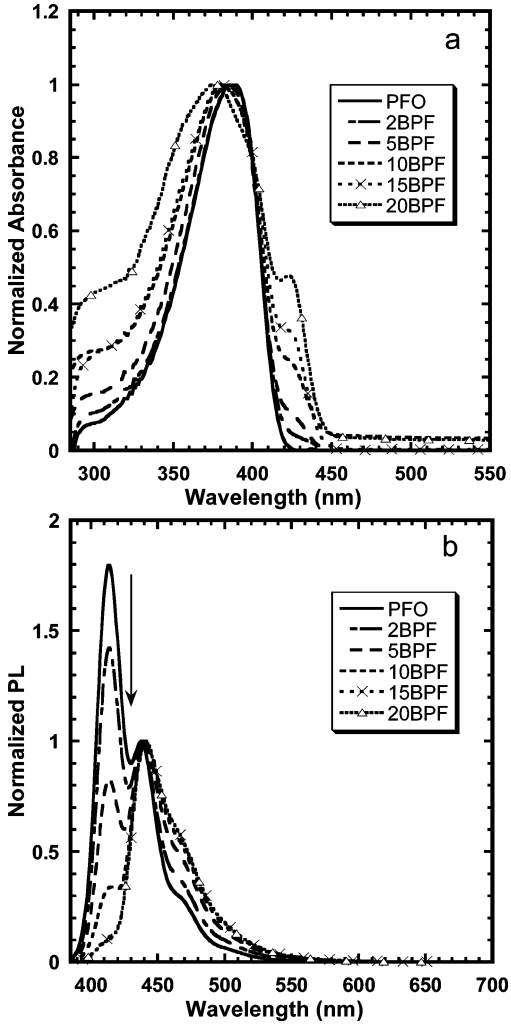

Figure 3. (a) Normalized optical absorption and (b) normalized PL emission (380 nm excitation) spectra of 10^{-5} M solutions of PFO and BPF copolymers in toluene.

PFO in cyclohexane.[15] Clearly, such aggregation cannot be expected at the dilute copolymer concentrations (10^{-5} M) in toluene in the present study. We believe that this 423 nm band is related to an intramolecular charge-transfer (ICT) transition[7] between donor fluorene and acceptor dibenzophenazine moieties. We note that such a red-shifted absorption band was not observed in the previously reported quinoxaline−fluorene copolymers.[3e]

Figure 3b shows the PL emission spectra of PFO and the five copolymers in 10^{-5} M toluene solutions, normalized relative to the 0−1 vibronic peak. The PL spectrum of PFO shows the typical blue emission with peaks at 414 and 438 nm, corresponding to the 0−0 and 0−1 vibronic transitions, respectively. As the dibenzophenazine content in the copolymer increases, the 0−1 peak steadily decreases and the broad emission in the 450−500 nm region increases. In 2BPF, the dominant emission peak is the 0−0 transition at 414 nm; in all the other copolymers, the 0−1 transition at 440 nm becomes the dominant emission band. We note that such a quenching of the 0−0 transition was observed in the PL emission spectra of QXF copolymers.[3e] The PL emission spectrum of 3,6-dibromodibenzo[*a*,*c*]phenazine in dilute toluene solution (not shown) had a peak at 410 nm and a tail extending up to 500 nm. The broad low-energy emission observed in the current copolymers is likely due to ICT effects. To confirm this hypothesis, we also investigated the dilute solution photophysics of PFO homopolymer and BPF copoly-

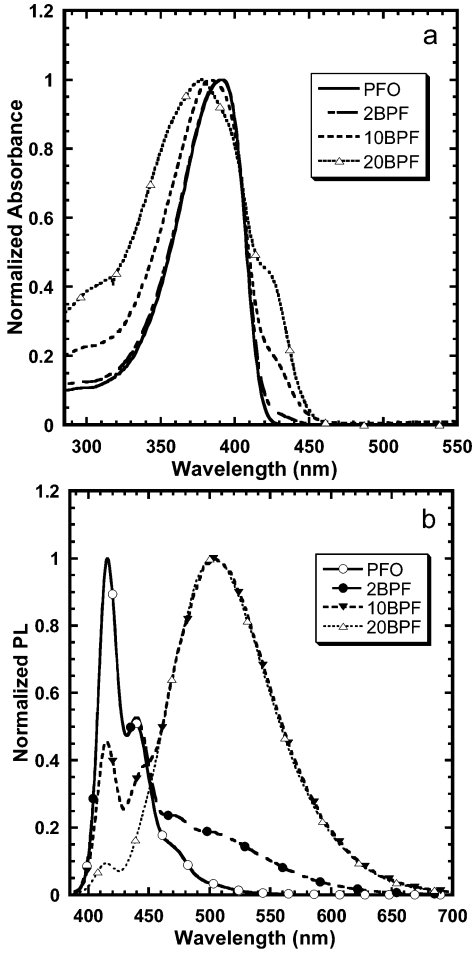

Figure 4. (a) Normalized optical absorption and (b) normalized PL emission (380 nm excitation) spectra of 10^{-5} M solutions of PFO and BPF copolymers in chloroform.

mers in chloroform, which has a higher dielectric constant ($\epsilon = 4.81$) compared to that of toluene ($\epsilon = 2.38$).[16]

Figure 4a shows the normalized optical absorption spectra of PFO, 2BPF, 10BPF, and 20BPF in dilute (10^{-5} M) chloroform solutions. These spectra are almost identical to the absorption spectra in toluene solutions. A gradual blue-shift and broadening of the main absorption band (~385 nm) is observed with increasing dibenzophenazine content from 2 to 20 mol %. PFO had its main band at 391 nm and 20BPF had a peak at 377 nm. The low-energy absorption band is at ~425 nm, similar to that at 423 nm in toluene. The absorption onsets are also identical in both solvents. Thus, the ground-state electronic structures of the copolymers are not much affected by the polarity of the solvent, suggesting a small dipole moment associated with the ICT transition.

Much larger differences were observed in the PL emission spectra of the copolymers in the two solvents. Figure 4b shows the normalized PL spectra of PFO, 2BPF, 10BPF, and 20BPF in dilute (10^{-5} M) chloroform solutions. The PL emission spectrum of PFO is similar to that in toluene solution, with the two well-resolved peaks at 416 and 439 nm. The PL emission spectrum of 2BPF also had two peaks at 416 and 440 nm; however, it also had a broad low-energy emission in the 480−600 nm region, which was not as intense in toluene solution (Figure 3b). This broad low-energy emission is dramatically enhanced in 10BPF, with an emission maximum of 502 nm; the blue band at 416 nm is quenched to ~45% of the intensity of the 502-nm band. In 20BPF, the blue band is further suppressed to ~10% of the intensity of the dominant 502 nm emission peak. Such a huge red-shift in the copolymer emission in the polar environment of chloroform is clearly indicative of an ICT excited state with a large dipole moment.[7a,9b] Charge-transfer excited states have been observed in an alternating fluorene copolymer containing a strong electron donor, triarylamine.[8a] In the current copolymers, the presence of the strong electron-accepting dibenzo[*a*,*c*]phenazine moieties on the polyfluorene chains leads to the observed ICT effects on the PL emission. This also supports our previous assignment of the ~420 nm absorption band in the BPF copolymers to an ICT transition. The absence of any such new low-energy absorption bands in the previously investigated quinoxaline−fluorene copolymers can be understood in terms of the much weaker electron-accepting strength of quinoxaline relative to dibenzo-[*a*,*c*]phenazine.

Increased excited-state ICT character is known to reduce the PL quantum yield (ϕ_f) of emissive conjugated copolymers.[7a,8] The estimated ϕ_f values of the current polymers in 10^{-5} M toluene solutions were 0.85, 0.80, 0.54, 0.47, 0.43, and 0.43 for PFO, 2BPF, 5BPF, 10BPF, 15BPF, and 20BPF, respectively. These ϕ_f values are quite similar compared to those of corresponding quinoxaline−fluorene copolymers that contained 2−50 mol % of quinoxaline moieties.[3e] For example, 15BPF has a ϕ_f value of 0.43, while 15QXF had a ϕ_f value of 0.48. Thus, the much stronger ICT interaction in the current BPF copolymers apparently does not quench their PL quantum yields as much, at least in solution. Overall, there is a 50% decrease in the ϕ_f value in going from 0 to 20 mol % of dibenzo[*a*,*c*]-phenazine in the copolymers due to the increased ICT effects with increasing acceptor moiety concentration. The photophysical properties of all the copolymers are summarized in Table 2.

The normalized optical absorption spectra of thin films of PFO and the five copolymers are shown in Figure 5a. The observed trends in terms of the spectral shifts and peak positions with increasing dibenzo[*a*,*c*]phenazine content in the copolymers are similar to the absorption spectra in dilute solutions. The main absorption band blue-shifts from 389 nm in PFO to 378 nm in 20BPF. The intensity of the low-energy band at ~430 nm increases with increasing dibenzophenazine content from PFO to 20BPF. The thin film spectra are broader compared to the solution spectra due to the extended delocalization and distribution in conjugation lengths in the solid state. The low-energy absorption at ~430 nm in PFO thin film is the commonly observed β-phase of PFO, which is comprised of a sequence of intrachain-ordered dioctylfluorene units.[17] In the BPF copolymers, one may also be tempted to assign the ~430 nm band to the β-phase of PFO. However, the same low-energy absorption band was also observed in dilute BPF solutions, where it was assigned to an ICT transition. Although the two transitions overlap here, there is no doubt that the 430 nm band in the BPF copolymers is the ICT absorption transition, and not the β-phase of PFO. The overall similarity between the thin film and dilute solution absorption spectra suggests similar ground-state electronic structures of the BPF copolymers in the two environments.

The PL emission spectra of the copolymer thin films under 380 nm excitation are shown in Figure 5b. The PFO spectrum has three vibronic transitions at 435, 460, and 490 nm, leading to deep-blue emission (CIE = 0.15, 0.06). All the BPF copolymers have red-shifted emission spectra relative to PFO. The PL spectra broaden with increasing dibenzo[*a*,*c*]phenazine content, and they red-shift steadily with emission maximum

Table 2. Photophysical Properties of Polymers

polymer	$\lambda_{a,max}$[a] in solution (nm)	$\lambda_{f,max}$[b] in solution (nm)	Φ_f[c]	$\lambda_{a,max}$[a] in thin film (nm)	$\lambda_{f,max}$[b] in thin film (nm)	CIE (*x*, *y*)[d]
PFO	387	414	0.85	389	435	(0.15, 0.06)
2BPF	386	414	0.80	388	451	(0.15, 0.15)
5BPF	385	440	0.54	387	460	(0.15, 0.19)
10BPF	382	441	0.47	384	468	(0.15, 0.23)
15BPF	380	441	0.43	383	472	(0.15, 0.24)
20BPF	378	441	0.43	378	474	(0.15, 0.28)

[a] The absorption maximum in toluene solution or in thin film. [b] The PL emission maximum in toluene solution or in thin film. [c] PL quantum yield in 10^{-5} M toluene solution. [d] CIE coordinates of thin film PL emission spectra.

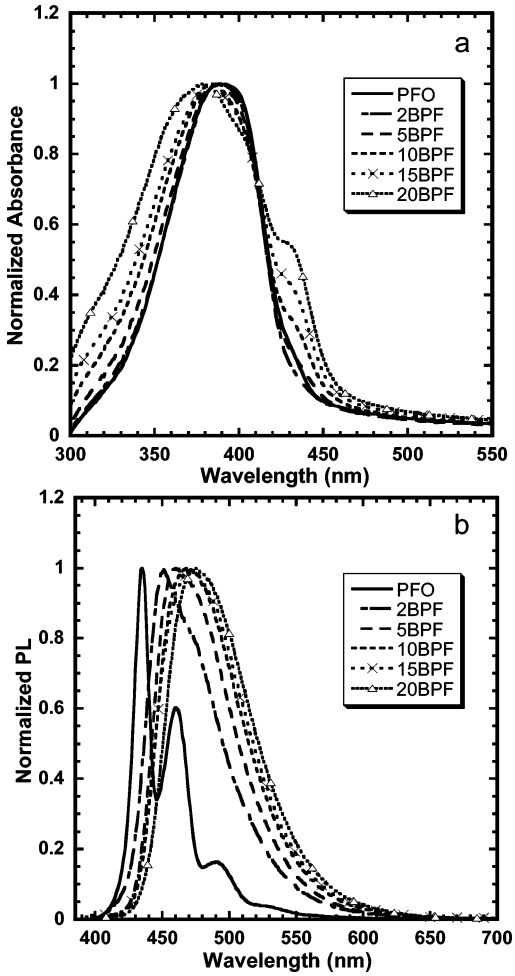

Figure 5. (a) Normalized optical absorption and (b) normalized PL emission (380 nm excitation) spectra of thin films of PFO and BPF copolymers.

ranging from 451 nm (2BPF) to 474 nm (20BPF). Both effects are due to increasing ICT character of the excited state in going from 2BPF to 20BPF, as previously discussed. As a result of this red-shift, the CIE emission coordinates vary from (0.15, 0.15) in 2BPF to (0.15, 0.28) in 20BPF. Overall, the thin film fluorescence from all the copolymers appears blue to the eye although the CIE-*y* coordinate approaches the blue-green region, particularly in 15BPF and 20BPF. No such red-shifted emissions were observed in thin films of the quinoxaline−fluorene copolymers.[3e] The larger ICT effects due to the presence of the stronger electron-accepting dibenzo[*a*,*c*]phenazine moieties in the current copolymers explain the observed red-shifted PL emissions in the BPF copolymers.

Electroluminescent Properties. Parts a−e of Figure 6 show the normalized EL spectra of type I diodes (ITO/PEDOT/Polymer/LiF/Al) based on PFO and the BPF copolymers. The EL emission color stays blue over the operating voltage range of the diodes for all the copolymers with no variation in the CIE coordinates. Table 3 summarizes the EL properties of the type I diodes. The PFO homopolymer has a deep-blue EL emission (CIE = 0.16, 0.07) with EL emission maximum at 434 nm. In each of the copolymers, the EL emission maximum is blue-shifted compared to the thin film PL spectrum (Figure 5b). For example, the EL emission maximum of 15BPF (Figure 6e) is at 452−455 nm over the operating voltage range, while its PL emission maximum is at 472 nm. The reason for the observed blue-shift is not clear. The EL emission spectra became narrower by up to 20 nm, as clearly seen in Figure 6d and e, with increasing applied voltage. Overall, the CIE coordinates of the EL emission of all the copolymers lie within the blue region as shown in Figure 6f.

The current density−electric field and luminance−voltage characteristics of the type I diodes are shown in Figure 7, parts a and b, respectively. At the same electric fields, the currents passing through the copolymer devices were generally lower than the PFO homopolymer diode, particularly at high fields of >2 MV/cm. This suggests a higher charge (electron) trapping and a better charge recombination efficiency in the copolymers due to the presence of the electron-accepting dibenzophenazine moieties. The variation in the brightness of the LEDs as a function of applied voltage is shown in Figure 7b. The PFO homopolymer diode had a maximum brightness of 198 cd/m^2 and a maximum luminous efficiency of 0.04 cd/A (Table 3). The best performance among the copolymers was given by 2BPF, with a brightness of 400 cd/m^2. The maximum brightness decreased from 400 cd/m^2 in 2BPF to ∼100 cd/m^2 in 20BPF diodes. This decreasing trend in device performance with increasing dibenzophenazine concentration matches very well with the observed variation in the PL quantum efficiencies of the copolymers (Table 2).

The addition of a buffer layer such as PVK, which serves as a hole-transport/electron-blocking layer, may increase the device efficiencies. The possible doping or protonation at the PEDOT/copolymer interface that could quench the luminescence of the emissive copolymers[18] would also be eliminated by adding such a buffer layer. We thus fabricated type II diodes with the architecture ITO/PEDOT/PVK/polymer/LiF/Al. The EL spectra of these diodes (not shown) were very similar to the corresponding type I diodes (Figure 6). Table 4 summarizes the relevant EL properties of type II devices. The device performance was not much different from the type I diodes. The main difference was in the 10BPF and 15BPF diodes, which had factors of 6−8 higher luminous efficiencies compared to their type I diodes. The best performance among the copolymers was given by 10BPF; all the copolymers had higher luminous efficiencies than the PFO homopolymer. Overall, we note that the maximum brightnesses and efficiencies obtained with these copolymers are comparable to those reported previously for quinoxaline−fluorene copolymer devices.[3e]

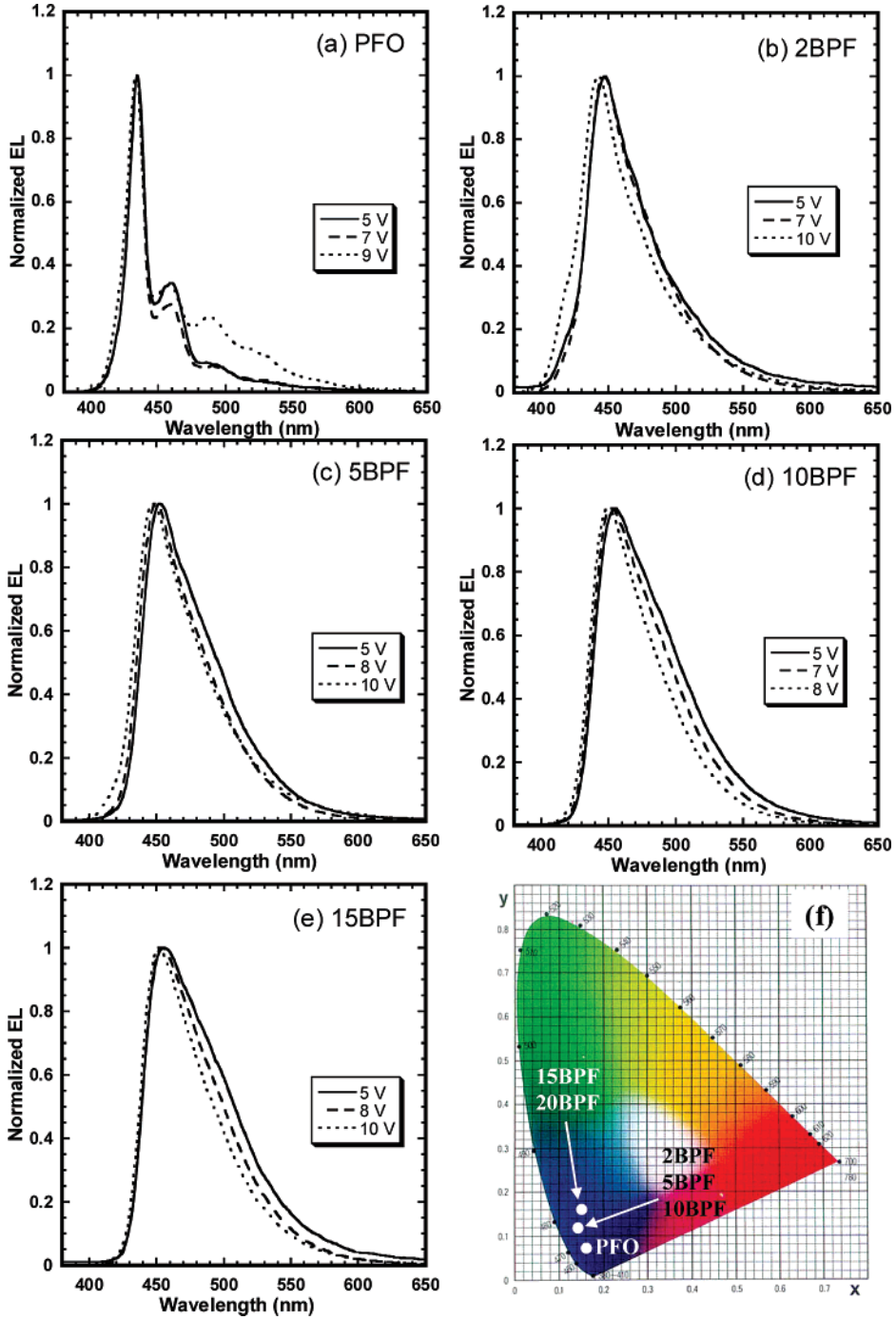

Figure 6. Normalized EL spectra of LEDs of the type ITO/PEDOT/Polymer/LiF/Al: (a) PFO, (b) 2BPF, (c) 5BPF, (d) 10BPF, and (e) 15BPF. (f) Plot of the CIE coordinates of the LEDs at their maximum efficiency.

To further increase the device efficiencies, a 20 nm thick TPBI electron-injection/hole-blocking layer was added in the type III diodes (ITO/PEDOT/PVK/polymer/TPBI/LiF/Al). All the device characteristics are collected in Table 5. As expected, the EL spectra of these diodes (not shown) were similar to the corresponding type I and II diodes, with emission arising solely from the copolymer layer. The EL emission maximum in each copolymer exactly matched its PL maximum, unlike the type I diodes where the EL spectra were blue-shifted. As a result, the CIE coordinates of the EL emission of the type III diodes match fairly well with the PL emission coordinates (Table 2) for each copolymer. At the higher applied voltages, a small peak around 370 nm appeared in the EL spectra due to emission from TPBI layer. This EL band was, however, less than 5% of the intensity of the dominant emission band and thus did not affect the CIE emission coordinates at all.

Parts a and b of Figure 8 show the current density−electric field and luminance−voltage characteristics of the type III diodes, respectively. The currents passing through all the copolymer devices are similar at the same electric fields. At fields >1.5 MV/cm, much higher currents pass through the copolymer diodes than the PFO device. Improvement in electron injection and transport due to the presence of the TPBI layer likely causes these increased current densities. Figure 8b shows the variation in the brightness of the LEDs as a function of applied voltage. The maximum luminances of all the devices are significantly higher than the corresponding types I and II diodes. The PFO homopolymer diode had a maximum bright-

Table 3. Device Characteristics of Type I LEDs: ITO/PEDOT/Polymer/LiF/Al[a]

polymer	drive voltage V (V)	current density J (mA/cm^2)	luminance L (cd/m^2)	luminous efficiency (cd/A)	EQE (%)	CIE (x, y)
PFO	8.45	500	198	0.04	0.048	(0.16, 0.10)
	7.5	*233*	*103*	*0.04*	*0.078*	*(0.16, 0.07)*
2BPF	10.55	500	401	0.08	0.105	(0.15, 0.11)
	8.4	*118*	*127*	*0.11*	*0.119*	*(0.15, 0.11)*
5BPF	10.00	500	260	0.05	0.051	(0.15, 0.12)
	8.00	*130*	*108*	*0.08*	*0.082*	*(0.14, 0.12)*
10BPF	8.60	497	248	0.05	0.049	(0.14, 0.12)
	8.00	*364*	*203*	*0.06*	*0.055*	*(0.14, 0.12)*
15BPF	9.60	500	159	0.03	0.027	(0.15, 0.14)
	8.40	*313*	*129*	*0.04*	*0.034*	*(0.15, 0.16)*
20BPF	8.55	364	102	0.03	0.023	(0.15, 0.16)
	8.25	*323*	*100*	*0.03*	*0.025*	*(0.15, 0.16)*

[a] Values in italics correspond to those for maximum luminous efficiencies at a brightness of ≥100 cd/m^2.

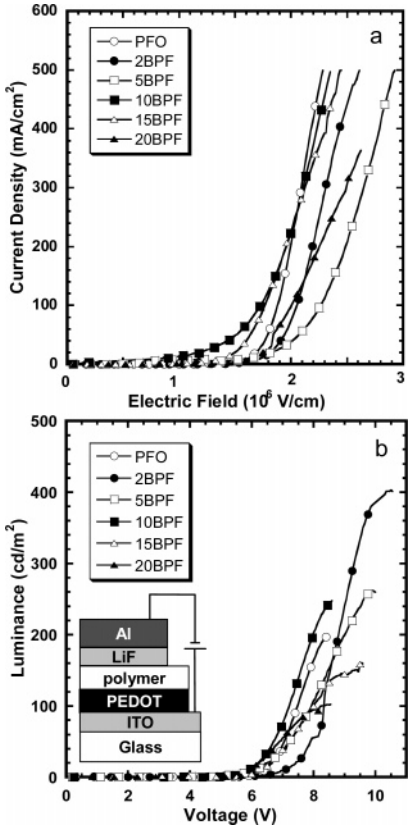

Figure 7. (a) Current density-electric field characteristics of type I polymer LEDs. (b) Luminance-voltage characteristics of the type I polymer LEDs. Inset shows the device schematic.

ness of 1956 cd/m^2, a maximum luminous efficiency of 1.3 cd/A, and an external quantum efficiency (EQE) of 1.94% at 126 cd/m^2 (Table 5). Except for 20BPF, all the other copolymers had superior device performance than the homopolymer diode. 2BPF gave the best performance with a maximum brightness of 4603 cd/m^2, a maximum luminous efficiency of 2.7 cd/A, and an EQE of 2.89% at 108 cd/m^2 (CIE = 0.15, 0.11). Thus, enhancements in brightness and efficiencies by factors of 2 are achieved in copolymer 2BPF relative to the PFO homopolymer, without compromising the blue color CIE coordinates. The observed trends in the device performance wth increasing dibenzo[*a*,*c*]phenazine content are similar to the type I diodes. Overall, the devices with TPBI (type III) had the best performance, with up to 20 times higher EQEs and over 10 times higher brightnesses than devices of type I or II architecture.

The variation in the luminous efficiency of the devices versus luminance is shown in Figure 8c. It is clear that all the BPF copolymers have higher brightnesses and efficiencies than the PFO homopolymer, except 20BPF. The efficiencies decrease by up to 50% from their maximum values at the maximum luminance of each copolymer device. This suggests imbalanced charge injection and recombination at the higher drive voltages. Further optimization of the relative film thicknesses may improve the charge balance and lead to nearly flat efficiency versus luminance curves. The luminous efficiencies steadily decrease with increasing dibenzo[*a*,*c*]phenazine content in the copolymers, largely a result of the corresponding decrease in their PL quantum yields (Table 2). The maximum luminous efficiency of 2.69 cd/A and maximum EQE of 2.89% at 108 cd/m^2 with blue CIE coordinates of (0.15, 0.11) in the 2BPF diode are comparable to the best blue polymer LEDs based on fluorescent emitters.[3,11a,19]

Figure 9 shows the variations in the diode maximum luminous efficiencies with dibenzo[*a*,*c*]phenazine content in the copolymer for all three device architectures. In the simplest type I diodes, all the efficiencies are well below 0.2 cd/A; 2BPF had the maximum efficiency of 0.11 cd/A (Table 3). In type II diodes, the efficiencies improved slightly; 10BPF had the best performance, with a maximum of 0.28 cd/A (Table 4). The efficiencies significantly increased upon the incorporation of the TPBI layer in type III diodes. The variation with copolymer composition is similar to type I devices. 2BPF had the maximum efficiency of 2.69 cd/A, while 20BPF had the lowest (0.74 cd/A), even lower than the PFO homopolymer (1.34 cd/A) (Table 5). The observed variation in the efficiencies for type III LEDs is in accord with the decrease in PL quantum yields of the copolymers with increasing dibenzophenazine content. A factor of 2 enhancement in performance compared to PFO is observed for 2BPF, likely due to a better balance in charge carrier injection and transport. Both PFO and 2BPF have very similar PL quantum yields (Table 2). On the other hand, 10BPF has a ∼50% lower PL quantum yield than PFO; however, a type III diode based on 10BPF has a higher efficiency of 1.71 cd/A relative to PFO (1.34 cd/A). Thus, the incorporation of the electron-deficient dibenzo[*a*,*c*]phenazine moiety in the predominantly p-type PFO backbone certainly improves the electron injection/transport and charge recombination efficiency. It appears that 2 mol % dibenzo[*a*,*c*]phenazine is the optimum copolymer composition. These results demonstrate that composition is a powerful tool to optimize the properties of EL copolymers and that dibenzo[*a*,*c*]phenazine is a promising new n-type building block for developing future organic semiconductors for optoelectronic applications.

Conclusions

We have synthesized five random dioctylfluorene−dibenzo[*a*,*c*]phenazine copolymers containing 2−20 mol % of the

Table 4. Device Characteristics of Type II LEDs: ITO/PEDOT/PVK/Polymer/LiF/Al[a]

polymer	drive voltage *V* (V)	current density *J* (mA/cm^2)	luminance *L* (cd/m^2)	luminous efficiency (cd/A)	EQE (%)	CIE (*x*, *y*)
PFO	12.00	448	91	0.02	0.03	(0.17, 0.19)
2BPF	10.40	357	357	0.10	0.12	(0.15, 0.10)
	8.85	*108*	*140*	*0.13*	*0.17*	*(0.15, 0.10)*
5BPF	8.20	241	162	0.07	0.07	(0.15, 0.12)
	7.65	*145*	*111*	*0.08*	*0.08*	*(0.15, 0.13)*
10BPF	8.80	269	466	0.17	0.14	(0.15, 0.17)
	7.15	*54*	*151*	*0.28*	*0.21*	*(0.15, 0.18)*
15BPF	9.25	142	324	0.23	0.18	(0.16, 0.16)
	9.20	*140*	*321*	*0.23*	*0.19*	*(0.16, 0.16)*
20BPF	9.10	84	73	0.09	0.06	(0.17, 0.20)

[a] Values in italics correspond to those for maximum luminous efficiencies at a brightness of ≥100 cd/m^2.

Table 5. Device Characteristics of Type III LEDs: ITO/PEDOT/PVK/Polymer/TPBI/LiF/Al[a]

polymer	drive voltage *V* (V)	current density *J* (mA/cm^2)	luminance *L* (cd/m^2)	luminous efficiency (cd/A)	EQE (%)	CIE (*x*, *y*)
PFO	11.30	261	1956	0.75	0.79	(0.17, 0.12)
	6.90	*9*	*126*	*1.34*	*1.94*	*(0.16, 0.08)*
2BPF	9.95	354	4603	1.30	0.94	(0.16, 0.19)
	7.10	*4*	*108*	*2.69*	*2.89*	*(0.15, 0.11)*
5BPF	10.50	357	3166	0.89	0.63	(0.16, 0.19)
	7.85	*16*	*351*	*2.15*	*1.92*	*(0.15, 0.14)*
10BPF	10.45	434	2972	0.68	0.42	(0.18, 0.24)
	7.50	*11*	*194*	*1.71*	*1.16*	*(0.16, 0.21)*
15BPF	10.00	283	2636	0.93	0.65	(0.16, 0.20)
	8.15	*35*	*474*	*1.36*	*0.90*	*(0.15, 0.22)*
20BPF	9.50	270	1263	0.47	0.31	(0.17, 0.23)
	7.75	*42*	*307*	*0.74*	*0.47*	*(0.17, 0.23)*

[a] Values in italics correspond to those for maximum luminous efficiencies at a brightness of ≥100 cd/m^2.

electron-deficient dibenzo[*a*,*c*]phenazine moiety and used them to achieve efficient blue electroluminescence from intramolecular charge-transfer excited states. The presence of the dibenzo[*a*,*c*]phenazine moieties in the copolymers led to intramolecular charge transfer states that were detected in optical absorption, photoluminescence, and electroluminescence spectra. Efficient blue electroluminescence was achieved from copolymer LEDs, with luminances of 1260−4600 cd/m^2 and external quantum efficiencies of 0.47−2.89% (at >100 cd/m^2) that varied with the copolymer composition. Enhanced brightnesses and efficiencies, compared to PFO homopolymer, were obtained in the copolymers due to the improved electron injection/transport properties and charge recombination efficiency because of the presence of the dibenzo[*a*,*c*]phenazine moiety. The copolymer containing 2 mol % dibenzo[*a*,*c*]phenazine gave the best performance with a maximum brightness of 4600 cd/m^2, a maximum luminous efficiency of 2.69 cd/A, an external quantum efficiency of 2.89% at 108 cd/m^2 and blue CIE coordinates of (0.15, 0.11), which is comparable to the best blue polymer LEDs. These results clearly demonstrate that dibenzo[*a*,*c*]phenazine is a promising n-type building block for developing organic semiconductors for electronics and optoelectronics.

Experimental Section

Materials. All starting materials and reagents were purchased from Aldrich and were used without further purification.

3,6-Dibromo-phenanthrene-9,10-dione (1). This compound was prepared by following a reported method.[20] Orange crystals, mp 290.1−290.8 °C. ^{1}H NMR ($CDCl_3$), δ (ppm): 8.14 (s, 2H), 8.09 (d, 2H), 7.70 (d, 2H). MS (FAB): Found M, 366.5, $C_{14}H_6Br_2O_2$ requires M, 366.0.

3,6-Dibromo-dibenzo[*a*,*c*]phenazine (2). This compound was prepared by following a reported method.[13] Yellow needles, mp 321.2−322 °C. ^{1}H NMR (CF_3COOD), δ (ppm): 9.10 (d, 2H), 8.76 (s, 2H), 8.67 (d, 2H), 8.35 (d, 2H), 8.06 (d, 2H). MS (EI): Found M, 437.8, $C_{20}H_{10}Br_2N_2$ requires M, 438.1.

Polymerization. The following general procedure was used for the preparation of all the copolymers and PFO homopolymer. To a three-necked flask was added 9,9-dioctylfluorene-2,7-bis(trimethyleneboronate) (558.4 mg, 1 mmol), 2,7-dibromofluorene and 3,6-dibromo-dibenzo[*a*,*c*]phenazine (total 1 mmol), Aliquat 336 (110.4 mg) and toluene (15 mL). Once all the monomers were dissolved, 2 M aqueous sodium carbonate solution (10 mL) was added. The flask equipped with a condenser was then evacuated and filled with argon several times to remove traces of air. Pd(PPh_3)$_4$ (15 mg, 0.013 mmol) was then added under an argon atmosphere. The mixture was then stirred for 48 h at 110 °C under argon. At the end of polymerization, the terminal boronic ester and bromine groups were sequentially end-capped by first refluxing for 12 h with bromobenzene (345 mg, 2.2 mmol) and then 12 h with phenylboronic acid (268 mg, 2.2 mmol). The reaction mixture was cooled to room temperature and the organic layer was separated, washed with water, and precipitated into methanol. The crude polymer was filtered, washed with excess methanol, and dried. The fibrous polymer was purified by a Soxhlet extraction in acetone for 2 days. The resultant polymer was further purified by dissolving in THF and reprecipitating into methanol several times. The pure copolymers were obtained after drying under vacuum at 50 °C overnight (yield, 62−76%).

PFO Homopolymer. ^{1}H NMR ($CDCl_3$), δ (ppm): 7.85 (b, 2H), 7.70 (b, 4H), 2.15 (b, 4H), 1.16 (b, 20H), 0.84 (m, 10H). FT−IR (film, cm^{-1}): 3018, 2926, 2852, 1459, 1253, 885, 813, 756.

20BPF Copolymer. ^{1}H NMR ($CDCl_3$), δ (ppm): 9.55 (b, 0.5H), 9.00 (b, 0.5H), 8.39 (b, 0.5H), 8.11 (b, 0.5H), 7.68−7.86 (m, 6.5H), 2.15 (b, 4H), 1.14 (b, 20H), 0.80 (b, 10H). FT−IR (film, cm^{-1}): 3059, 3028, 2926, 2853, 1607, 1532, 1460, 1403, 1358, 1254, 1140, 1067, 883, 760.

Other copolymers had NMR and FT−IR spectra that were similar to those of 20BPF copolymer, except that the relative intensities of signals are different due to the different composition of the copolymer.

Characterization. FT−IR spectra were taken on a Perkin-Elmer 1720 FTIR spectrophotometer with NaCl plates. ^{1}H NMR spectra were recorded on a Bruker-DRX499 or Bruker-AF300 spectrometer at 500 and 300 MHz, respectively. Melting points were determined

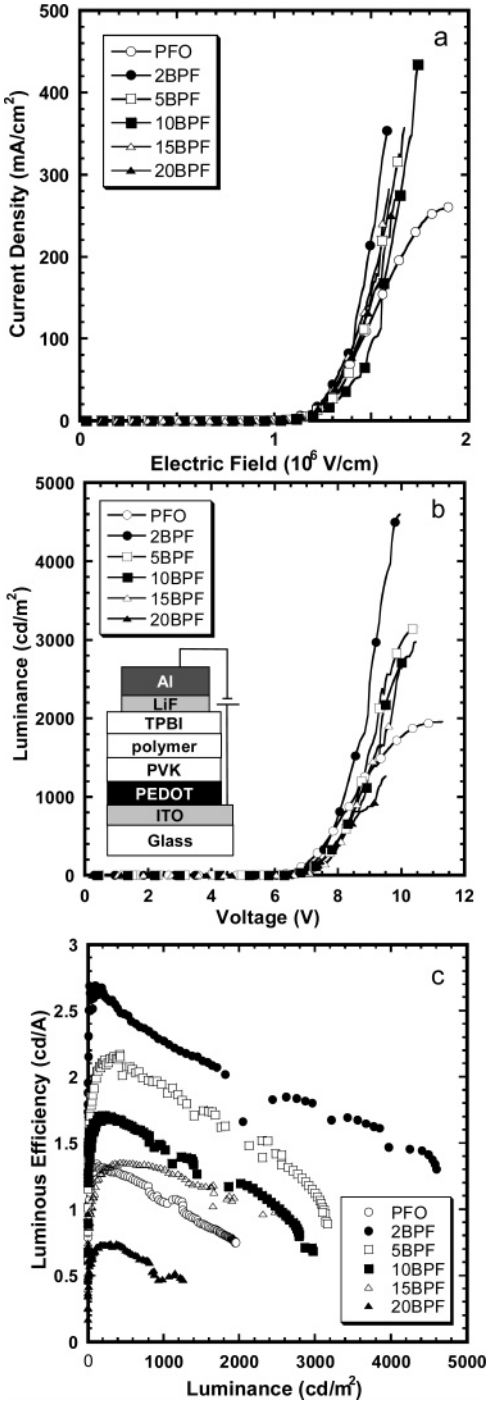

Figure 8. (a) Current density-electric field characteristics of type III polymer LEDs. (b) Luminance-voltage characteristics of the type III polymer LEDs. Inset shows the device schematic. (c) Luminous efficiency as a function of the luminance of the diodes.

on an Electrothermal IA9100 digital melting point instrument at a heating rate of 1 °C/min. Gel permeation chromatography (GPC) analysis of the polymers was performed on a Waters gel permeation chromatograph with Shodex gel columns and Waters model 150 C refractive index detectors using THF as eluent and polystyrene standards as reference. Differential scanning calorimetry (DSC) analysis was performed on a TA instrument Q100 DSC under N_2 at a heating rate of 10 °C/min, and thermogravimetric analysis (TGA) analysis was conducted with a TA instrument Q50 TGA at a heating rate of 20 °C/min under a nitrogen gas flow. Optical absorption spectra were taken on a Perkin-Elmer model Lambda 900 Uv/vis/near-IR spectrophotometer. PL emission spectra were obtained on a Photon Technology International (PTI) Inc. model QM-2001-4 spectrofluorimeter. To measure the PL quantum yields

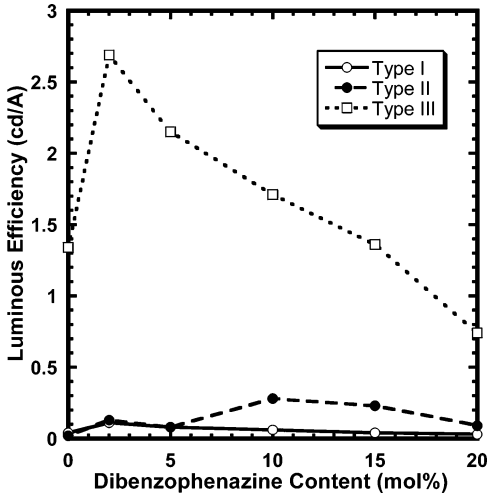

Figure 9. Maximum luminous efficiency of the polymer LEDs vs dibenzo[*a*,*c*]phenazine content in the copolymers for the three device architectures.

(Φ_f), polymer solutions in spectral grade toluene were prepared. The concentration ($\sim 10^{-5}$ M) was adjusted so that the absorbance of the solution would be lower than 0.1. A 10^{-5} M solution of 9,10-diphenylanthracene in toluene ($\Phi_f = 0.93$) was used as a standard.[21] All solutions were purged with nitrogen for 15 min before spectral acquisition.

Fabrication and Characterization of LEDs. ITO-coated glass substrates (Delta Technologies Ltd., Stillwater, MN) were cleaned sequentially in ultrasonic bathes of detergent solution, deionized water, chloroform, isopropanol, deionized water, and finally, acetone. After drying the ITO substrates overnight at 60 °C in a vacuum, a 65 nm thick poly(ethylenedioxythiophene)/poly(styrene sulfonate) blend (PEDOT) hole injection layer was spin-coated on top of ITO and dried at 200 °C for 15 min under a vacuum. Before spin-coating, the as-received PEDOT solution was diluted by ~25% with 1:1 (v/v) water/isopropanol and was then filtered through 0.45 μm PVDF syringe filters. Three types of OLEDs were fabricated with the copolymers as the emissive material, poly(*N*-vinylcarbazole) (PVK) as the hole-transport/electron-blocking layer and 1,3,5-tris(*N*-phenylbenzimidizol-2-yl)benzene (TPBI) as the electron-transport/hole-blocking layer: Type I ITO/PEDOT/polymer/LiF/Al, Type II ITO/PEDOT/PVK/polymer/LiF/Al, and Type III ITO/PEDOT/PVK/polymer/TPBI/LiF/Al. PVK was spin-coated from its 0.5 wt % solution in toluene to give a 20 nm thick film on PEDOT. The film was dried in a vacuum at 60 °C overnight. Thin films of PFO or the copolymers were obtained by spin-coating on top of PEDOT or PVK from ~1 wt % solutions in toluene and dried in a vacuum at 60 °C overnight. Before spin-coating, all the solutions were filtered through 0.2 μm PTFE syringe filters. The thickness of the copolymer films on glass was measured by a Alpha-Step 500 Surface Profiler (KLA Tencor, Mountain View, CA) to be between 33 and 40 nm. Because of the partial solubility of PVK in toluene, the interface between PVK and the copolymers is not flat; the total thickness of the composite PVK/copolymer bilayers was measured to be between 38 and 42 nm. 20 nm thick films of TPBI were obtained by evaporation from resistively heated quartz crucibles at a rate of ~0.2 nm/s in a vacuum evaporator (Edwards Auto 306) at base pressures of $<9 \times 10^{-7}$ Torr. The chamber was vented with air to load the cathode materials, pumped back down, and then a 2 nm LiF and a ~120 nm thick aluminum layer were sequentially deposited through a shadow mask without breaking vacuum to form active diode areas of 0.2 cm^2. To record the current−voltage data, we used an HP4155A semiconductor parameter analyzer (Yokogawa Hewlett-Packard, Tokyo) and the luminance was measured simultaneously with a model 370 optometer (UDT Instruments, Baltimore, MD) equipped with a calibrated sensor head (model 211) and a 5× objective lens. The device external quantum efficiencies were calculated using procedures

reported previously.[2e,3e,22] All the device fabrication and characterization were done under ambient laboratory conditions.

Acknowledgment. This research was supported by the NSF (grant CTS-0437912), the Air Force Office of Scientific Research (grant F49620-03-1-0162), and the NSF STC MDITR (DMR-0120967).

References and Notes

(1) (a) Neher, D. *Macromol. Rapid Commun.* **2001**, *22*, 1365. (b) Scherf, U.; List, E. J. W. *Adv. Mater.* **2002**, *14*, 477. (c) Leclerc, M. *J. Polym. Sci., Part A: Polym. Chem.* **2001**, *39*, 2867. (d) Becker, S.; Ego, C.; Grimsdale, A. C.; List, E. J. W.; Marsitzky, D.; Pogantsch, A.; Setayesh, S.; Leising, G.; Müllen, K. *Synth. Met.* **2002**, *125*, 73. (e) Chen, P.; Yang, G.; Liu, T.; Li, T.; Wang, M.; Huang, W. *Polym. Int.* **2006**, *55*, 473. (f) Kulkarni, A. P.; Tonzola, C. J.; Babel, A.; Jenekhe, S. A. *Chem. Mater.* **2004**, *16*, 4556.

(2) (a) Millard, I. S. *Synth. Met.* **2000**, *111*−*112*, 119. (b) Wu, W.; Inbasekaran, M.; Hudack, M.; Welsh, D.; Yu, W.; Cheng, Y.; Wang, C.; Kram, S.; Tacey, M.; Bernius, M.; Fletcher, R.; Kiszka, K.; Munger, S.; O'Brien, J. *Microelectron. J.* **2004**, *35*, 343. (c) Liao, L. S.; Fung, M. K.; Lee, C. S.; Lee, S. T.; Inbasekaran, M.; Woo, E. P.; Wu, W. W. *Appl. Phys. Lett.* **2000**, *76*, 3582. (d) Kulkarni, A. P.; Jenekhe, S. A. *Macromolecules* **2003**, *36*, 5285. (e) Kulkarni, A. P.; Kong, X.; Jenekhe, S. A. *J. Phys. Chem. B* **2004**, *108*, 8689.

(3) (a) Hung, M.-C.; Liao, J.-L.; Chen, S.-A.; Chen, S.-H.; Su, A.-C. *J. Am. Chem. Soc.* **2005**, *127*, 14576. (b) Li, J. Y.; Ziegler, A.; Wegner, G. *Chem.*−*Eur. J.* **2005**, *11*, 4450. (c) Xin, Y.; Wen, G.-A.; Zeng, W.-J.; Zhao, L.; Zhu, X.-R.; Fan, Q.-L.; Feng, J.-C.; Wang, L.-H.; Wei, W.; Peng, B.; Cao, Y.; Huang, W. *Macromolecules* **2005**, *38*, 6755. (d) Shu, C.-F.; Dodda, R.; Wu, F.-I.; Liu, M. S.; Jen, A. K.-Y. *Macromolecules* **2003**, *36*, 6698. (e) Kulkarni, A. P.; Zhu, Y.; Jenekhe, S. A. *Macromolecules* **2005**, *38*, 1553.

(4) (a) Muller, C. D.; Falcou, A.; Reckefuss, N.; Rojahn, M.; Wiederhirn, V.; Rudati, P.; Frohne, H.; Nuyken, O.; Becker, H.; Meerholz, K. *Nature* **2003**, *421*, 829. (b) Herguth, P.; Jiang, X.; Liu, M. S.; Jen, A. K.-Y. *Macromolecules* **2002**, *35*, 6094. (c) Wu, W.-C.; Liu, C.-L.; Chen, W.-C. *Polymer* **2006**, *47*, 527. (d) Beaupre, S.; Leclerc, M. *Adv. Funct. Mater.* **2002**, *12*, 192. (e) Yang, R.; Tian, R.; Yan, J.; Zhang, Y.; Yang, J.; Hou, Q.; Yang, W.; Zhang, C.; Cao, Y. *Macromolecules* **2005**, *38*, 244.

(5) (a) Zhang, F.; Perzon, E.; Wang, X.; Mammo, W.; Andersson, M. R.; Inganas, O. *Adv. Funct. Mater.* **2005**, *15*, 745. (b) Svensson, M.; Zhang, F. Veenstra, S. C.; Verhees, W. J. H.; Hummelen, J. C.; Kroon, J. M.; Inganäs, O.; Andersson, M. R. *Adv. Mater.* **2003**, *15*, 988. (c) Yu, G.; Gao, J.; Hummelen, J. C.; Wudl, F.; Heeger, A. J. *Science* **1995**, *270*, 1789. (d) Brabec, C. J.; Winder, C.; Sariciftci, N. S.; Hummelen, J. C.; Dhanabalan, A.; Van Hal, P. A.; Janssen, R. A. J. *Adv. Funct. Mater.* **2002**, *12*, 709. (e) Sonmez, G.; Shen, C. K. F.; Rubin, Y.; Wudl, F. *Adv. Mater.* **2005**, *17*, 897. (f) Jenekhe, S. A.; Yi, S. *Appl. Phys. Lett.* **2000**, *77*, 2635. (g) Alam, M. M.; Jenekhe, S. A. *J. Phys. Chem. B* **2001**, *105*, 2479. (h) Alam, M. M.; Jenekhe, S. A. *Chem. Mater.* **2004**, *16*, 4647.

(6) (a) Chen, M.; Crispin, X.; Perzon, E.; Andersson, M. R.; Pullerits, T.; Andersson, M.; Inganäs, O.; Berggren, M. *Appl. Phys. Lett.* **2005**, *87*, 252105. (b) Babel, A.; Jenekhe, S. A. *Macromolecules* **2003**, *36*, 7759. (c) Redecker, M.; Bradley, D. D. C.; Inbasekaran, M.; Woo, E. P. *Appl. Phys. Lett.* **1998**, *73*, 1565. (d) Champion, R. D.; Cheng, K.-F.; Pai, C.-L.; Chen, W.-C.; Jenekhe, S. A. *Macromol. Rapid Commun.* **2005**, *26*, 1835. (e) Babel, A.; Wind, J. D.; Jenekhe, S. A. *Adv. Funct. Mater.* **2004**, *14*, 891. (f) Yamamoto, T.; Yasuda, T.; Sakai, Y.; Aramaki, S. *Macromol. Rapid Commun.* **2005**, *26*, 1214. (g) Yamamoto, T.; Kokubo, H.; Kobashi, M.; Sakai, Y. *Chem. Mater.* **2004**, *16*, 4616. (h) Yasuda, T.; Sakai, Y.; Aramaki, S.; Yamamoto, T. *Chem. Mater.* **2005**, *17*, 6060.

(7) (a) Jenekhe, S. A.; Lu, L.; Alam, M. M. *Macromolecules* **2001**, *34*, 7315. (b) van Mullekom, H. A. M.; Vekemans, J. A. J. M.; Havinga, E. E.; Meijer, E. W. *Mater. Sci. Eng., R* **2001**, *32*, 1.

(8) (a) Redecker, M.; Bradley, D. D. C.; Baldwin, K. J.; Smith, D. A.; Inbasekaran, M.; Wu, W. W.; Woo, E. P. *J. Mater. Chem.* **1999**, *9*, 2151. (b) Thompson, B. C.; Madrigal, L. G.; Pinto, M. R.; Kang, T.-S.; Schanze, K. S.; Reynolds, J. R. *J. Polym. Sci., Part A: Polym. Chem.* **2005**, *43*, 1417. (c) Tonzola, C. J.; Alam, M. M.; Jenekhe, S. A. *Adv. Mater.* **2002**, *14*, 1086. (d) Tonzola, C. J.; Alam, M. M.; Bean, B. A.; Jenekhe, S. A. *Macromolecules* **2004**, *37*, 3554.

(9) (a) Zhu, Y.; Kulkarni, A. P.; Jenekhe, S. A. *Chem. Mater.* **2005**, *17*, 5225. (b) Kulkarni, A. P.; Wu, P.-T.; Kwon, T. W.; Jenekhe, S. A. *J. Phys. Chem. B* **2005**, *109*, 19584. (c) Kulkarni, A. P.; Kong, X.; Jenekhe, S. A. *Adv. Funct. Mater.* **2006**, *16*, 1057. (d) Hancock, J. M.; Gifford, A. P.; Zhu, Y.; Lou, Y.; Jenekhe, S. A. *Chem. Mater.* **2006**, *18*, 4924.

(10) (a) Thomas, K. R. J.; Lin, J. T.; Tao, Y.-T.; Chuen, C.-H. *Chem. Mater.* **2002**, *14*, 3852. (b) Chiang, C.-L.; Wu, M.-F.; Dai, D.-C.; Wen, Y.-S.; Wang, J.-K.; Chen, C.-T. *Adv. Funct. Mater.* **2005**, *15*, 231. (c) Shirota, Y.; Kinoshita, M.; Noda, T.; Okumoto, K.; Ohara, T. *J. Am. Chem. Soc.* **2000**, *122*, 11021.

(11) (a) Wu, F.-I.; Reddy, S.; Shu, C.-F.; Liu, M. S.; Jen, A. K.-Y. *Chem. Mater.* **2003**, *15*, 269. (b) Zhan, X.; Liu, Y.; Wu, X.; Wang, S.; Zhu, D. *Macromolecules* **2002**, *35*, 2529. (c) Yang, W.; Huang, J.; Liu, C.; Niu, Y.; Hou, Q.; Yang, R.; Cao, Y. *Polymer* **2004**, *45*, 865.

(12) Tabner, B. J.; Yandle, J. R. *J. Chem. Soc. A* **1968**, 381.

(13) Kato, S.; Hashimoto, H.; Hida, M.; Maezawa, M. *Yuki Gosei Kagaku Kyokaishi* **1957**, *15*, 399.

(14) Grell, M.; Bradley, D. D. C.; Inbasekaran, M.; Woo, E. P. *Adv. Mater.* **1997**, *9*, 798.

(15) Grell, M.; Bradley, D. D. C.; Long, X.; Chamberlain, T.; Inbasekaran, M.; Woo, E. P.; Soliman, M. *Acta Polym.* **1998**, *49*, 439.

(16) Reichardt, C. *Solvents and Solvent Effects in Organic Chemistry*; Verlag Chemie: New York, 1988.

(17) Grell, M.; Bradley, D. D. C.; Ungar, G.; Hill, J.; Whitehead, K. S. *Macromolecules* **1999**, *32*, 5810.

(18) (a) Kim, J.-S.; Ho, P. K. H.; Murphy, C. E.; Seeley, A. J. A. B.; Grizzi, I.; Burroughes, J. H.; Friend, R. H. *Chem. Phys. Lett.* **2004**, *386*, 2. (b) Peisert, H.; Knupfer, M.; Zhang, F.; Petr, A.; Dunsch, L.; Fink, J. *Appl. Phys. Lett.* **2003**, *83*, 3930.

(19) (a) Weinfurtner, K.-H.; Fujikawa, H.; Tokito, S.; Taga, Y. *Appl. Phys. Lett.* **2000**, *76*, 2502. (b) Liu, J.; Min, C.; Zhou, Q.; Cheng, Y.; Wang, L.; Ma, D.; Jing, X.; Wang, F. *Appl. Phys. Lett.* **2006**, *88*, 083505. (c) Lee, Y. K.; Kwon, S. K.; Kang, M. H.; Kim, J. Y.; Park, T. J.; Song, D. H.; Jang, J.; Jin, J. K.; Shin, D. C.; Choi, W. J.; You, H.; Kim, Y. H.; Kwon, S. K.; Kwon, J. H.; Yang, N. C. *SID Int. Symp. Dig. Tech. Pap.* **2005**, *36*, 858.

(20) Kato, S.; Hida, M.; Uehara, S.; Hara, J. *Yuki Gosei Kagaku Kyokaishi* **1957**, *15*, 84.

(21) Heinrich, G.; Schoof, S.; Gusten, H. *J. Photochem.* **1974**, *3*, 315.

(22) (a) Zhang, X.; Shetty, A. S.; Jenekhe, S. A. *Macromolecules* **1999**, *32*, 7422. (b) Zhang, X.; Jenekhe, S. A. *Macromolecules* **2000**, *33*, 2069.

MA062445Z